Thermal Decomposition of HO_2NO_2 (Peroxynitric Acid, PNA): Rate Coefficient and Determination of the Enthalpy of Formation

Tomasz Gierczak,[†,‡,§] **Elena Jiménez,**[†,‡,||] **Veronique Riffault,**[†,‡] **James B. Burkholder,**[†] **and A. R. Ravishankara***[†,⊥]

Aeronomy Laboratory, National Oceanic and Atmospheric Administration, 325 Broadway, Boulder, Colorado 80305-3328, and Cooperative Institute for Research in Environmental Sciences, University of Colorado, Boulder, Colorado 80309

Received: July 28, 2004; In Final Form: October 23, 2004

Rate coefficients for the gas-phase thermal decomposition of HO_2NO_2 (peroxynitric acid, PNA) are reported at temperatures between 331 and 350 K at total pressures of 25 and 50 Torr of N_2. Rate coefficients were determined by measuring the steady-state OH concentration in a mixture of known concentrations of HO_2NO_2 and NO. The measured thermal decomposition rate coefficients $k_{-1}(T,P)$ are used in combination with previously published rate coefficient data for the HO_2NO_2 formation reaction to yield a standard enthalpy for reaction 1 of $\Delta_r H°_{298\,K} = -24.0 \pm 0.5$ kcal mol^{-1} (uncertainties are 2σ values and include estimated systematic errors). A HO_2NO_2 standard heat of formation, $\Delta_f H°_{298\,K}(HO_2NO_2)$, of -12.6 ± 1.0 kcal mol^{-1} was calculated from this value. Some of the previously reported data on the thermal decomposition of HO_2NO_2 have been reanalyzed and shown to be in good agreement with our reported value.

1. Introduction

Peroxynitric acid (HO_2NO_2, PNA) plays an important role in atmospheric chemistry as a gas-phase reservoir for NO_x (=NO and NO_2) and HO_x (=OH and HO_2) in both the stratosphere and troposphere.[1] HO_2NO_2 is not directly emitted into the atmosphere but is formed via the association reaction of HO_2 with NO_2

$$HO_2 + NO_2 + M \leftrightarrow HO_2NO_2 + M \qquad (1, -1)$$

thereby providing a link between the HO_x and NO_x families of reactive species. The dominant atmospheric loss processes for HO_2NO_2 consist of thermal decomposition,[2−4] photodissociation (UV and visible/near-IR),[5−8] and reaction with the OH radical.[9,10] The contribution of each of these processes to the total loss rate of HO_2NO_2 depends greatly on the location and time. The lifetime of HO_2NO_2 at middle latitudes in the upper troposphere and lower stratosphere is in the range of 10−20 h. However, at the higher temperatures found in the lower troposphere and even the middle to upper stratosphere, HO_2NO_2 loss can be dominated by thermal decomposition (reaction −1). Therefore, our understanding of the chemistry of HO_2NO_2 in the atmosphere from the Earth's surface up to the lower stratosphere requires an accurate accounting of its thermal decomposition kinetics.

Graham et al.[2,3] and, more recently, Zabel[4] have examined the thermal decomposition kinetics of HO_2NO_2 via laboratory studies. They measured the rate of disappearance of HO_2NO_2 in the presence of excess NO using Fourier transform infrared absorption in large-volume reaction chambers between 261 and 295 K and at pressures of 1−760 Torr, N_2 or O_2. The measured loss rate coefficient, attributed to thermal decomposition, depended on both the total pressure and temperature.

The thermochemical parameters for HO_2NO_2 have been determined through a second-law (van't Hoff) analysis of the calculated equilibrium constant for reaction 1 obtained using independently measured forward and reverse rate coefficients and the reported thermochemical data for HO_2 and NO_2. Sander and Peterson[11] used their measurements of $k_1(T,P)$ and the thermal decomposition results from Graham et al. to derive $\Delta_r H°_{298\,K} = -23.0$ kcal mol^{-1} and $\Delta_r S°_{298\,K} = 37.9$ cal K^{-1} mol^{-1}, leading to $\Delta_f H°_{298\,K}(HO_2NO_2) = -12.6 \pm 2.0$ kcal mol^{-1} ($\Delta_r H°$ = enthalpy of reaction; $\Delta_r S°$ = entropy of reaction; $\Delta_f H°$ = heat of formation). Subsequently, Zabel[4] combined his thermal decomposition rate coefficients and $k_1(T,P)$ from Kurylo and Ouellette[12] to derive $\Delta_r H°_{298\,K} = -23.8 \pm 0.7$ kcal mol^{-1} and $\Delta_r S°_{298\,K} = 40.7 \pm 2.6$ cal K^{-1} mol^{-1}. In this paper, we will use the third-law method to analyze our data because in the van't Hoff method there is a strong correlation between $\Delta_r H°_{298\,K}$ and $\Delta_r S°_{298\,K}$ (see the Results and Discussion section). More recently, Regimbal and Mozurkewich[13] measured the thermal decomposition of HO_2NO_2 in an aqueous solution with a $CuSO_4$ catalyst using a spectro-iodometric method. They quote a value for the gas-phase standard heat of formation of HO_2NO_2 of -12.9 ± 0.6 kcal mol^{-1}. Their value for $\Delta_f H°_{298\,K}(HO_2NO_2)$ provides the basis for the current value quoted by Sander et al.[14] However, a gas-phase determination of $\Delta_f H°_{298\,K}(HO_2NO_2)$ and the rate coefficients for the thermal decomposition of HO_2NO_2 are still desired.

In this work, a different experimental approach using pulsed laser photolysis with laser induced fluorescence (LIF) detection of the OH radical was applied to measure gas-phase HO_2NO_2 thermal decomposition rate coefficients between 330 and 350

---

* To whom correspondence should be addressed. E-mail: A.R.Ravishankara@noaa.gov.

[†] National Oceanic and Atmospheric Administration.

[‡] University of Colorado.

[§] Permanent address: Department of Chemistry, Warsaw University, ul. Zwirki i Wigury 101, 02-089 Warsaw, Poland.

[||] Current address: Departamento de Química Física, Facultad de Ciencias Químicas, Universidad de Castilla−La Mancha, Camilo José Cela 10, 13071 Ciudad Real, Spain.

[⊥] Also associated with the Department of Chemistry and Biochemistry, University of Colorado, Boulder, CO 80309.

10.1021/jp046632f CCC: $30.25

K and 25 and 50 Torr of N_2. The use of a different measurement method provided a means to minimize potential systematic errors. The measured thermal decomposition rate coefficients were used in combination with literature values of $k_1(T,P)$ (measured over the same temperature and pressure ranges) and $\Delta_r S°_{298\,K}$ for reaction 1 (calculated using statistical thermodynamics) to determine $\Delta_r H°_{298\,K}$ and $\Delta_f H°_{298\,K}(HO_2NO_2)$. Some of the previously reported data are reanalyzed and shown to be consistent with our values.

2. Experimental Details

The experimental approach that we used to determine the thermal decomposition rate coefficient of HO_2NO_2 differs significantly from the methods used in previous studies. In our approach, NO was added to HO_2NO_2 (in equilibrium with HO_2 and NO_2), initiating the following gas-phase reactions:

$$HO_2 + NO \rightarrow OH + NO_2 \tag{2}$$

$$OH + X \rightarrow \text{products} \tag{3}$$

In reaction 3, X represents all of the species in the gas mixture (HO_2NO_2, NO, NO_2, and H_2O_2) that react with OH. The OH radical concentration was described by the rate equation

$$d[OH]/dt = \text{production rate} - \text{loss rate} \tag{I}$$

In excess NO, where HO_2 is immediately converted to OH,

$$d[OH]/dt = k_{-1}[HO_2NO_2] - k_3'[OH] \tag{II}$$

where $k_3' = k_3[X]$. The reaction system rapidly reaches steady-state in OH, $d[OH]/dt = 0$, and eq II yields the HO_2NO_2 thermal decomposition rate coefficient $k_{-1}(T,P)$ in terms of k_3', $[OH]_{ss}$, and $[HO_2NO_2]$, which are each experimentally measurable quantities.

$$k_{-1}(T,P) = (k_3'[OH]_{ss})/[HO_2NO_2] \tag{III}$$

A key requirement for the applicability of this approach is that OH must be in steady-state. This condition was evaluated using numerical simulations of the rate equations and was verified experimentally, as will be shown in the Results and Discussion section. A numerical simulation of the OH temporal profile in the presence of NO and HO_2NO_2, using the rate coefficients given in Table 1 and concentrations representative of our experimental conditions, is shown in Figure 1. For this calculation, only HO_2NO_2, NO_2, and NO were present initially. The calculation shows that, in less than 0.5 ms, HO_2NO_2 was close to its equilibrium value (reaction 1, −1) and that, within 2 ms, the OH radical reached a steady-state concentration. At $t = 0$, the OH and HO_2 concentrations were instantaneously perturbed. Experimentally, the perturbation resulted from the 248 nm pulsed laser photolysis of HO_2NO_2, H_2O_2, and HNO_3 in the gas mixture. The OH concentration initially increased following the conversion of HO_2 to OH (reaction 2) and decayed by reaction 3. Within several milliseconds, dependent on the value of k_3', the [OH] returned to its initial steady-state concentration, $[OH]_{ss}$. Through these simple model calculations, we have demonstrated that a steady-state OH concentration should be established rapidly everywhere in the reactor with a value representative of the temperature (HO_2NO_2 thermal decomposition rate coefficient) of that location in the reactor.

The following sections describe the experimental details of the LIF apparatus and the techniques used in the determination of temperature, k_3', $[OH]_{ss}$, and $[HO_2NO_2]$. The experimental apparatus used for the determination of $k_{-1}(T,P)$ was nearly the same as that used in our recent study of the kinetics of the OH + HO_2NO_2 reaction.[10] A schematic of the experimental apparatus is shown in Figure 2. The key features of the apparatus included (1) a source of gas-phase HO_2NO_2, (2) a Fourier transform infrared spectrometer used for the determination of the HO_2NO_2, H_2O_2, NO_2, and HNO_3 concentrations prior to entering the reaction cell, (3) a temperature-regulated reaction cell where OH was measured via LIF, (4) a diode array spectrometer used for UV absorption measurements and quantification of the HO_2NO_2 concentration after the reaction cell (in some experiments the optical path was through the reaction cell, as described below), and (5) a 248 nm excimer laser used for the photolysis of the HO_2NO_2 gas mixture and perturbation of the steady-state OH radical concentration.

TABLE 1: Reaction Mechanism Used in Numerical Simulations[a]

reaction	$k(T)^b$ (cm^3 $molecule^{-1}$ s^{-1})
Thermal Decomposition	
$HO_2NO_2 + M \rightarrow HO_2 + NO_2 + M$	this work[c]
Hydroxyl Radical Reactions	
$OH \rightarrow$ loss	250[c,d]
$OH + PNA \rightarrow H_2O + O_2 + NO_2$	$8.8 \times 10^{-19} T^2 \exp(1130/T)$[e]
$OH + PNA \rightarrow HO_2 + HNO_3$	
$OH + PNA \rightarrow H_2O_2 + NO_3$	
$OH + H_2O_2 \rightarrow HO_2 + H_2O$	$2.9 \times 10^{-12} \exp(-110/T)$[e]
$OH + NO_2 + M \rightarrow HNO_3 + M$	1.4×10^{-12}
$OH + HNO_3 \rightarrow H_2O + NO_3$	1.0×10^{-13}
$OH + NO + M \rightarrow HONO + M$	6.2×10^{-13}
$OH + HONO \rightarrow H_2O + NO_2$	$1.8 \times 10^{-11} \exp(-390/T)$
HO_2 Radical Reactions	
$HO_2 + NO_2 + M \rightarrow HO_2NO_2 + M$	1.4×10^{-13}
$HO_2 + NO \rightarrow OH + NO_2$	$3.5 \times 10^{-12} \exp(250/T)$
$HO_2 + HO_2 + M \rightarrow H_2O_2 + O_2 + M$	1.3×10^{-12}
NO_3 Radical Reactions	
$NO_3 + NO \rightarrow 2\ NO_2$	$1.5 \times 10^{-11} \exp(-170/T)$
$NO_3 + NO_2 + M \rightarrow N_2O_5 + M$	4.5×10^{-13}
$NO_3 + HO_2 \rightarrow OH + NO_2 + O_2$	3.5×10^{-12}

[a] Unless noted, the rate coefficients are taken from Sander et al.[14] [b] Pressure-dependent rate coefficients are for 50 Torr of N_2 at 340 K. [c] Units: s^{-1}. [d] Typical first-order loss rate coefficient measured in this work. [e] Jimenez et al.[10]

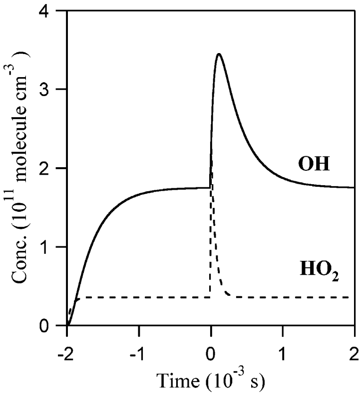

Figure 1. Numerical simulation of the temporal profile of OH (solid line) and HO_2 (dashed line) in the presence of NO and HO_2NO_2 using the reaction mechanism outlined in Table 1 with $T = 340$ K, $k_{-1}(T,P) = 1.1\ s^{-1}$, $[NO] = 2.1 \times 10^{15}$ molecules cm^{-3}, and $[HO_2NO_2] = 5.4 \times 10^{14}$ molecules cm^{-3}. The calculation demonstrates that OH and HO_2 rapidly reach steady-state concentrations and rapidly return to the same prephotolysis values following a pulsed photolysis perturbation.

The pulsed LIF apparatus has been extensively used in our laboratory[15] and is only briefly described here. OH radicals were detected by pulsed LIF by excitation at ∼282 nm from the

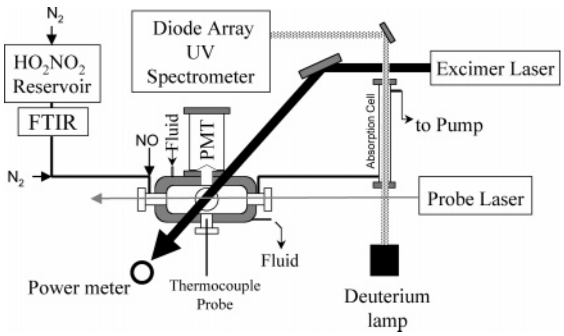

Figure 2. Schematic of the experimental apparatus used in the determination of $k_{-1}(T,P)$.

frequency-doubled output of a Nd:YAG-pumped dye laser (probe laser). The OH fluorescence signal was detected with a photomultiplier tube (PMT) that was oriented perpendicular to the probe beam. A band-pass filter (peak transmission at 309 nm; fwhm band-pass of 20 nm) that was mounted in front of the PMT was used to isolate the OH fluorescence. The PMT signal was fed into a gated charge integrator and then to a personal computer for data acquisition and analysis. The reactor consisted of a jacketed Pyrex reactor approximately 15 cm in length (along the axis of the gas flow) with an internal volume of ~150 cm^3. The detection limit for OH in this system, defined as $S/N = 1$, where S is the signal and N is equal to twice the standard deviation of the mean of the background signal, was ca. 2×10^9 molecules cm^{-3} in 100 Torr of N$_2$ for 100 laser shots.

The reactor was maintained at a constant temperature by circulating a fluid from a heating bath through its jacket. The temperature profile along the axis of the gas flow within the reactor was measured using a retractable calibrated thermocouple. The temperature of the gas mixture within the volume where the probe and excimer laser beams crossed each other (i.e., the location where $[OH]_{ss}$ was measured) was measured before and after each experiment using a retractable thermocouple, as shown in Figure 2. The thermocouple was fully retracted when the OH signal was measured. At the highest temperature of this study, the difference in temperature between the reactor wall and the center was 4 K. The gas flowing through the reactor essentially reached the reactor temperature within a couple of centimeters of entering it. The temperature of the reaction volume was accurate to 0.2 K.

2.1. $[OH]_{ss}$. The steady-state OH signal (S_{OH}^{PNA}) was measured using pulsed LIF in a mixture of HO$_2$NO$_2$, NO, and carrier gas. The determination of $[OH]_{ss}$ requires an absolute calibration of the LIF detection system. We used photolysis of H$_2$O$_2$ at 248 nm to create a known concentration of OH and signal. This signal was used to convert the measured S_{OH}^{PNA} to $[OH]_{ss}$ using the following formula:

$$[OH]_{ss} = \frac{S_{OH}^{PNA}}{S_{OH}^{H_2O_2}} \phi_{H_2O_2} \sigma_{248\ nm}^{H_2O_2} [H_2O_2] E f \qquad (IV)$$

where $S_{OH}^{H_2O_2}$ is the OH signal at $t = 0$ from H$_2$O$_2$ photolysis, $\Phi_{H_2O_2}$ is the quantum yield for OH from photolysis of H$_2$O$_2$ ($\Phi_{H_2O_2} = 2$), $\sigma_{248\ nm}^{H_2O_2}$ is the H$_2$O$_2$ absorption cross section at 248 nm (photolysis wavelength), E is the photolysis laser fluence (photons cm^{-2} pulse^{-1}) measured using a power meter, and f is the measured correction to account for the difference between laser fluence in the center of the reactor and that measured behind the reactor. In each experiment, the S_{OH}^{PNA} signal was measured approximately 10 times and the average value was used to calculate $[OH]_{ss}$. The values of $[OH]_{ss}$ were in the range $(0.1-4.0) \times 10^{11}$ molecules cm^{-3} during the course of our experiments.

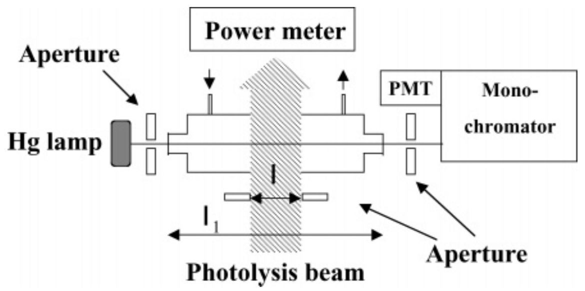

Figure 3. Schematic of the experimental setup used in the O$_3$ actinometry measurements.

2.1.1. Photolysis Laser Power Meter Calibration. The photolysis laser fluence was measured using a power meter at the exit of the LIF reactor, as shown in Figure 2. The power meter was calibrated using two independent actinometry methods using NO$_2$ and O$_3$ as reference compounds, as described separately below.

2.1.1.1. NO$_2$ Actinometry. Laser fluence (power meter) calibration using pulsed photolysis of NO$_2$ as a reference gas has been used in our laboratory previously and is described in detail by Gierczak et al.[16] Using a small volume absorption cell, a mixture of NO$_2$ in a N$_2$ buffer gas (ca. 90 Torr) was photolyzed by the excimer laser while monitoring the laser fluence with a power meter. The laser fluence ($F_{248\ nm}$) is determined from the slope of the loss of NO$_2$, monitored by UV absorption using a diode array spectrometer, as a function of the number of laser pulses (n):

$$\ln([NO_2]_0/[NO_2]_n) = (\sigma_{248\ nm}\Phi_{loss}F_{248\ nm})n \qquad (V)$$

where $\sigma_{248\ nm}$ is the NO$_2$ absorption cross section at 248 nm and Φ_{loss} is the quantum yield for NO$_2$ loss. In our experiments, [NO$_2$] was ca. 1×10^{16} molecules cm^{-3} and the laser fluences were in the range 1.3−12.7 mJ cm^{-2} pulse^{-1} (similar to those used in the thermal decomposition rate coefficient measurements). The quantum yield for NO$_2$ photolysis (Φ_{NO_2}) was assumed to be unity:

$$NO_2 + h\nu \rightarrow O + NO \qquad (4)$$

Under our conditions, the O atom generated in reaction 4 will react with NO$_2$:

$$O + NO_2 \rightarrow NO + O_2 \qquad (5)$$

resulting in $\Phi_{loss} = 2\Phi_{NO_2}$. The NO$_2$ absorption cross section at 248 nm was measured in this work, relative to its infrared peak cross section of 5.53×10^{-17} cm^2 molecule^{-1} at 1600 cm^{-1}, to be $(2.1 \pm 0.3) \times 10^{-20}$ cm^2 molecule^{-1}; this value is in reasonable agreement with the value reported by Schneider et al.,[17] $\sigma_{248\ nm} = (1.8 \pm 0.2) \times 10^{-20}$ cm^2 molecule^{-1}.

2.1.1.2. O$_3$ Actinometry. An extensive description of the O$_3$ actinometry at 248 nm is given elsewhere.[18] Briefly, we used a quartz cell that was positioned perpendicular to the photolysis beam and equipped with quartz windows (see Figure 3). The cell window facing the photolysis laser beam was covered with an aperture to precisely define the area of the photolysis beam that traversed the cell ($l = 3$ cm). A beam of UV radiation from a high pressure mercury lamp traversed through the quartz windows of the cell ($l_1 = 7$ cm) at a right angle to the 3 cm wide photolysis beam. A monochromator isolated the 254 nm radiation, and it was detected by a PMT. The output of the PMT was monitored using an oscilloscope. A mixture of O_3, N_2, and O_2 (total pressure = 200 Torr; 195 Torr of N_2 and 5 Torr of O_2) was flowed through the cell. N_2 was used to rapidly quench $O(^1D)$, produced by O_3 photolysis, to $O(^3P)$. Subsequently, $O(^3P)$ reacted with O_2 ($[O_2] \approx (4-16) \times 10^{16}$ molecules cm^{-3}) to re-form ozone. The PMT signal I_0 was measured prior to adding ozone, O_3 was introduced, and the signal level I_1 was measured. Once the signal was stable, the mixture was photolyzed. Photolysis of O_3 increased the PMT signal from I_1 to I_2 in a quick step, reflecting the loss of ozone ($[O_3]_{\text{lost}}$) in the photolysis beam. Then it relaxed to its previous value (I_1) as a result of the re-formation of O_3. We calculated $F_{248\text{ nm}}$ using the following equation:

$$F_{248\text{ nm}} = [\ln(I_0/I_2)l_1]/\sigma_{248}l \qquad \text{(VI)}$$

The absorption cross section of ozone at 248 nm ($\sigma_{248} = 1.07 \times 10^{-17}$ cm^2 molecule^{-1}) was taken from Sander et al.[14] The calculated laser fluence was corrected for the attenuation by the two quartz surfaces of the windows. The two methods of laser power meter calibration are in good agreement. In the final thermal decomposition rate coefficient data analysis, an average of the fluence calculated using the two methods was used.

2.2. [HO_2NO_2] Measurement. The HO_2NO_2 concentration was measured using two different optical methods; Fourier transform infrared absorption was used before the reactor, and diode array absorption was used after the reactor. The HO_2NO_2 concentration at the center of the reactor, where the OH radical concentration was measured, was derived from these measurements. Two different configurations were used for the UV absorption measurements. The first arrangement was identical to that used in our previous study of the OH + HO_2NO_2 reaction.[10] In this configuration, the UV absorption cell spanned the LIF reactor with equal optical path lengths on each side. This configuration presented a problem at the higher temperatures used in this study because of the significant losses of HO_2NO_2 in the reactor. In the second and preferred configuration, as shown in Figure 2, the UV absorption cell was positioned after the LIF reactor. This configuration enabled a direct measure of the loss of PNA in the reactor by comparing [HO_2NO_2] measured by UV absorption after the reactor with that measured before the reactor via infrared absorption.

2.2.1. Infrared Absorption Measurements. Infrared absorption spectra were measured at room temperature using a Fourier transform spectrometer. Spectra were recorded from 500 to 4000 cm^{-1} at 1 cm^{-1} resolution with 100 coadded scans. A 15 cm long Pyrex absorption cell with germanium windows was used for all measurements. The infrared band intensities used to quantify the HO_2NO_2 concentration were taken from Smith,[19] Smith et al.,[9] and our previous HO_2NO_2 study.[10] Infrared band intensities for NO_2, HNO_3, and H_2O_2 were taken from the HITRAN database.[20] The concentrations of HO_2NO_2, HNO_3, and H_2O_2 in the LIF reactor, derived from the IR absorption measurements, were corrected for calibrated dilution factors and pressure and temperature differences between the IR absorption cell and the reactor.

2.2.2. UV Absorption Measurements. UV absorption measurements used a 30 W D_2 lamp light source and a 1024 element diode array detector.[21] The spectrograph covered the wavelength range 200−450 nm with a resolution of ~1.5 nm. The absorption spectrum of a HO_2NO_2 sample recorded by a diode array spectrometer was the sum of the absorptions due to HO_2NO_2, NO_2, H_2O_2, and HNO_3. The accurate determination of the HO_2NO_2 concentration from the measured UV absorption spectrum was somewhat dependent on the concentration of NO_2, H_2O_2, and HNO_3 present in the sample (see Jiménez et al.[10] for details and examples). The H_2O_2 and HNO_3 contributions were calculated from their concentrations, which were measured using infrared absorption. UV absorption cross sections reported in the literature for HO_2NO_2,[22] H_2O_2,[14] and HNO_3[14] were used in the spectral analysis. NO_2 reference spectra were recorded under identical experimental conditions and using approximately the same NO_2 concentrations as observed in the thermal decomposition experiments. The contributions of H_2O_2 and HNO_3 to the total absorption signal near 250 nm were small; in most cases, they were less than 15% of the HO_2NO_2 absorption signal. The NO_2 absorption depended on the temperature and, therefore, the amount of HO_2NO_2 decomposition in the reactor. At the highest temperatures of our study, the concentration of NO_2 exceeded that of HO_2NO_2. The HO_2NO_2 concentration in the reactor was calculated using the pressure and temperature in this region and the HO_2NO_2 concentration measured in the absorption cells.

While using the first optical arrangement, which was only used when the loss of HO_2NO_2 in the reactor was small (<20%), the average of the HO_2NO_2 concentration measured by IR ($[HO_2NO_2]_{IR}$) and UV ($[HO_2NO_2]_{UV}$) was taken to be the concentration in the reactor. The second arrangement was used for the higher temperature measurements, where the loss of HO_2NO_2 in the reactor was larger (up to 80%). The concentration of HO_2NO_2 in the reaction zone inside the reactor was calculated assuming that [HO_2NO_2] decreased exponentially through the reactor.

2.3. k_3' Measurement. Laser photolysis was used to produce a pulse of OH. Measuring its temporal profile, as it returned to its prephotolysis steady-state concentration, yielded k_3'. The individual contributions to the OH decay rate coefficient need not be identified to extract the thermal decomposition rate coefficient; that is, the measured value of k_3' is used in the analysis. Values of k_3' ranged from 3 000 to 11 000 s^{-1} and were determined using a nonlinear least-squares fit of a biexponential expression to the OH temporal profile. Reaction with NO contributed the most to the measured value of k_3', followed by NO_2 and then PNA.

2.4. Materials. He (99.9999%), N_2 (>99.99%), and NO_2BF_4 were used as supplied. Concentrated hydrogen peroxide (>90%) was prepared by bubbling dry N_2 through an initially 60 wt % H_2O_2 sample for several days prior to use. The H_2O_2 purity was determined by titration with a standard solution of $KMnO_4$.

PNA was synthesized by slowly dissolving 3 g of NO_2BF_4 in 8 mL of H_2O_2 (>90%) while keeping the reaction mixture at 273 K.[10,23] HO_2NO_2 was introduced into the gas flow by passing a small flow of He over the HO_2NO_2 solution while maintaining the reservoir at 273 K. H_2O_2 was introduced into the apparatus by bubbling a calibrated N_2 flow through the H_2O_2 sample. Gas flow rates were measured using calibrated mass flow transducers. Pressures were measured using 100 and 1000 Torr capacitance manometers. Experiments were performed at total pressures of 25 and 50 Torr using N_2 as the carrier gas.

3. Results and Discussion

In this section we present (1) our measured values of $k_{-1}(T,P)$, the HO_2NO_2 thermal decomposition rate coefficient; (2) the determination of the thermodynamic quantities $\Delta_r H°_{298\text{ K}}$, $\Delta_r S°_{298\text{ K}}$, $\Delta_f H°_{298\text{ K}}(HO_2NO_2)$, and $S°_{298\text{ K}}(HO_2NO_2)$; (3) an error analysis undertaken to assess the uncertainties in the thermodynamic data derived in this work; and (4) a comparison with the results from previous studies.

TABLE 2: HO_2NO_2 Thermal Decomposition Rate Coefficient Measurement Conditions and Results

T (K)	P (Torr, N_2)	flow velocity (cm s^{-1})	$[NO_2]_{IR}$[a]	$[NO]_{reactor}$[a]	$[PNA]_{before}$[a,b]	$[PNA]_{after}$[a,c]	$[PNA]_{after}$/$[PNA]_{before}$	$[PNA]_{reactor}$[a,d]	$[OH]_{ss}$[a]	k_3' (s^{-1})	$k_{-1}(T,P)$ (s^{-1})
331.3	53.0	64	2.2	21	6.4	6.9[e]	1.08	6.6	3.0	5380	0.23
	51.7	65	5.7	36	5.7	6.4[e]	1.12	6.0	2.5	5920	0.24
	51.1	65	4.9	30	8.0	9.7[e]	1.21	8.9	2.6	6760	0.20
	52.4	67	3.7	29	3.1	3.3[e]	1.06	3.2	1.5	4390	0.20
	52.5	66	3.7	29	5.6	6.0[e]	1.07	5.8	2.2	5215	0.20
											0.21 ± 0.02[f]
331.7	25.0	99	3.9	22	9.1	7.5	0.82	8.3	4.2	5050	0.26
	25.0	99	2.2	22	8.8	7.0	0.79	7.9	4.7	5250	0.32
	25.0	99	1.9	22	8.2	6.5	0.80	7.3	5.2	4750	0.34
	25.0	104	2.8	20	4.3	2.9	0.67	3.6	4.2	2980	0.35
	25.1	104	1.5	20	6.5	4.6	0.71	5.4	6.3	3860	0.45
											0.34 ± 0.07[f]
334.4	51.8	63	4.8	37	7.4	7.15[e]	0.97	7.3	4.1	6620	0.37
	50.2	66	3.8	34	7.3	7.8[e]	1.07	7.6	4.1	6900	0.37
											0.37[f]
337.9	51.3	47	4.7	48	10.1	10.3[e]	1.02	10.2	8.2	9050	0.73
341.6	25.1	104	3.8	21	7.6	5.5	0.73	6.5	11.0	4640	0.79
	25.1	109	3.6	20	3.2	2.0	0.65	2.6	9.4	2890	1.06
	25.2	108	3.0	20	4.8	3.0	0.63	3.8	14.3	3040	1.14
	25.0	108	3.0	20	3.3	1.6	0.48	2.3	9.8	2860	1.22
	25.2	106	1.9	20	5.8	3.6	0.62	4.5	14.2	3460	1.08
											1.06 ± 0.16[f]
342.4	53.3	49	7.4	45	8.8	2.4	0.27	4.6	9.1	8540	1.69
	53.0	51	8.5	45	3.5	0.9	0.35	1.8	6.3	5630	2.02
	53.0	51	9.2	44	4.6	1.3	0.28	2.5	7.6	6185	1.91
	53.2	49	6.7	47	8.1	2.3	0.28	4.3	11.3	7500	1.97
	53.0	49	6.3	46	8.0	2.1	0.26	4.1	10.1	7195	1.78
											1.87 ± 0.14[f]
343.2	52.5	100	2.5	22	4.3	2.7	0.62	3.4	9.2	4365	1.17
	52.6	100	2.4	21	3.1	1.4	0.45	2.1	7.4	3360	1.20
	52.4	98	2.9	22	4.4	2.4	0.56	3.3	7.1	3780	0.82
	52.4	97	1.5	23	4.2	2.6	0.63	3.4	10.9	3680	1.19
											1.1 ± 0.18[f]
347.3	25.0	109	2.8	20	6.6	4.4	0.67	5.4	24.0	3680	1.63
	25.1	110	2.0	20	4.5	2.8	0.63	3.6	18.8	3200	1.69
	25.1	105	0.9	21	6.7	4.9	0.73	5.7	19.4	3430	1.17
	25.1	110	1.4	20	4.3	2.7	0.61	3.4	21.3	2150	1.35
	25.3	110	0.8	20	5.5	3.2	0.59	4.2	25.2	2550	1.53
											1.47 ± 0.21[f]
349.9	52.5	52	5.3	43	9.6	2.1	0.22	4.5	19.5	8260	3.60
	53.4	54	5.9	42	4.8	1.4	0.29	2.6	13.3	4910	2.47
	53.0	53	5.7	43	5.8	1.3	0.22	2.7	14.9	6030	3.29
	52.9	51	5.7	45	6.2	1.5	0.24	3.0	15.4	6730	3.43
	53.1	49	4.7	47	8.3	1.9	0.23	4.0	18.5	6675	3.12
											3.18 ± 0.44[f]

[a] $[HO_2NO_2]$, $[NO_2]$, and [NO] are in units of 10^{14} molecules cm^{-3}; [OH] are in units of 10^{10} molecules cm^{-3}. [b] $[HO_2NO_2]$ was measured by Fourier transform infrared absorption before entering the reactor. [c] $[HO_2NO_2]$ was measured by UV diode array absorption after the reactor unless noted. [d] $[PNA]_{reactor}$ was calculated (1) as an average of $[PNA]_{IR}$ and $[PNA]_{UV}$ for UV measurements made through the reactor or (2) assuming an exponential decay of HO_2NO_2 through the reactor (see text for details) for UV measurements made after the reactor. [e] $[HO_2NO_2]$ was measured by diode array absorption through the reactor. [f] Average $k_{-1}(T,P)$ value.

3.1. Measurement of $k_{-1}(T,P)$. The thermal decomposition rate coefficients $k_{-1}(T,P)$, measured in 25 and 50 Torr of N_2 between 331 and 350 K, are summarized in Table 2. A representative OH temporal profile used in the determination of $k_{-1}(T,P)$ is shown in Figure 4. The OH profile shows the key characteristics that were outlined in the numerical simulations that were described in the Experimental Section and shown in Figure 1. $[OH]_{ss}$ was measured prior to the photolysis experiment, and the values shown are only superimposed for comparison purposes. Following photolysis of the HO_2NO_2 gas mixture, the OH temporal profile is well represented by the biexponential fit shown in the figure, with the OH signal returning to the prephotolysis steady-state value. This is consistent with OH indeed being in steady-state prior to the photolysis pulse. Values of $k_{-1}(T,P)$ ranged from 0.20 s^{-1} at 331.3 K to 3.60 s^{-1} at 349.9 K. The determination of $k_{-1}(T,P)$ at a given temperature and pressure showed good reproducibility, with standard deviations on the order of 10−15%. A complete error analysis including estimated systematic errors is presented later.

The temperature range used in our study, 331.3−349.9 K, was established as a result of our ability to accurately determine $[OH]_{ss}$ and $[HO_2NO_2]_{reactor}$. $[OH]_{ss}$ decreases significantly with decreasing temperature. The low temperature limit was therefore established using the criteria that $[OH]_{ss}$ be greater than 1×10^{10} molecules cm^{-3} ($S/N \sim 5$). The highest temperature was established by the extent of HO_2NO_2 decomposition in the reactor. The determination of $[HO_2NO_2]$ in the center of the reactor required an accurate measure of $[HO_2NO_2]$ at the exit of the reactor. Separate measurements made with the entire apparatus at room temperature demonstrated that HO_2NO_2 losses outside of the heated reactor were insignificant. Therefore, the concentration analysis did not require any corrections to account for HO_2NO_2 losses outside of the reactor. Only experiments

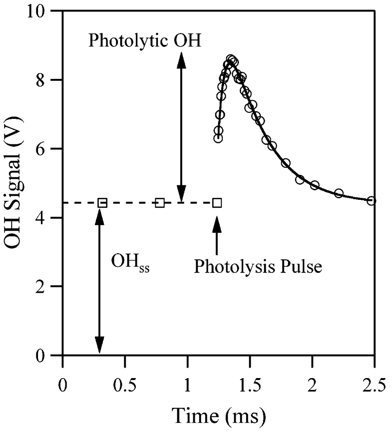

Figure 4. Experimentally measured OH radical temporal profile showing (1) the initial OH signal level (open squares and dashed line) measured prior to the pulsed photolysis experiment, (2) the OH signal following pulsed laser photolysis of the HO_2NO_2 sample at 248 nm (open circles), and (3) a biexponential nonlinear least-squares fit to the OH profile (solid line). This measurement was made at $T = 347.3$ K with $[HO_2NO_2] = 5.4 \times 10^{14}$ molecules cm^{-3}, $[NO] = 2.0 \times 10^{15}$ molecules cm^{-3}, $P = 25.0$ Torr of N_2, and a 248 nm photolysis laser fluence of 1.44 mJ cm^{-2} pulse^{-1}.

with a ratio value greater than 0.15 for $[HO_2NO_2]$ measured before and after the reactor were used in the final data analysis. For residence times in the reactor used in our measurements, this corresponded to a temperature of ~350 K.

$[HO_2NO_2]_{reactor}$ was calculated from the measured IR and UV absorption and is given in Table 2. At each temperature, $k_{-1}(T,P)$ was measured using several different $[HO_2NO_2]$; concentrations ranged from 3×10^{14} to 12×10^{14} molecules cm^{-3}. The measured $k_{-1}(T,P)$ values were found to be independent of $[HO_2NO_2]_{reactor}$. Although less accurate than the IR and UV absorption measurements, values of $[HO_2NO_2]_{reactor}$ were estimated from the measured magnitude of the OH signal, S_{OH}, and the first-order loss rate coefficient, k_3'. Photolysis of H_2O_2 and HNO_3, along with HO_2 from HO_2NO_2 photolysis, all contribute to the measured S_{OH}. A biexponential fit of the measured OH temporal profile following photolysis yields $[OH]_0$ and $[HO_2]_0$. However, using the measured concentration of H_2O_2, the OH signal from HO_2 produced from HO_2NO_2 photolysis could be estimated. We used our recently measured OH and HO_2 quantum yields in HO_2NO_2 photolysis at 248 nm.[8] Alternately, the first-order rate coefficient for OH loss in this reaction system, simply described by reaction 3, is due to the loss of OH via reaction with NO, NO_2, H_2O_2, HNO_3, and HO_2NO_2. Using the measured NO, NO_2, H_2O_2, and HNO_3 concentrations and our recently reported rate coefficient for the OH + HO_2NO_2 reaction,[10] we could estimate $[HO_2NO_2]_{reactor}$. In most cases, the $[HO_2NO_2]_{reactor}$ estimated from these two methods agreed (±30%) with those presented in Table 2. We note that $[HO_2NO_2]_{reactor}$ estimated using these indirect methods are less precise than the concentration determined by IR and UV absorption, but they do provide a valuable consistency test and an evaluation of possible systematic errors. The linear velocity of the gas through the reactor was also changed from 47 to 110 cm s^{-1} over the course of the experiments. Although the loss of HO_2NO_2 in the reactor was dependent on the residence time within the reactor, the determination of $k_{-1}(T,P)$ was not. This provides another indirect confirmation for our accuracy in determining $[HO_2NO_2]_{reactor}$.

3.2. Thermodynamics. The rate coefficients for HO_2NO_2 thermal decomposition obtained in this study were combined with the rate coefficients for the association of HO_2 with NO_2 (reaction 1) to obtain the equilibrium constant $K_c = k_1(T,P)/k_{-1}(T,P)$. For the present calculations, we took $k_1(T,P)$ values calculated using the "fall-off" parameters recommended by Sander et al.[14] These parameters were based on the work of Kurylo and Ouellette[12,24] at 25, 50, and 100 Torr of N_2 over the temperature range 358−228 K and Sander and Peterson[11] at higher pressures. These parameters reproduce the $k_1(T,P)$ data of Kurylo and Ouellette within 5% at the pressures and temperatures used in the present work. More recently, Christensen et al.[25] reported $k_1(T,P)$ values measured over the temperature range 220−298 K at 45−200 Torr of N_2. The "fall-off" parameters obtained in their work yielded $k_1(T,P)$ values in good agreement with earlier measurements carried out at the temperatures and pressures used in this study. It should be pointed out, however, that the analysis presented below can easily be updated when more accurate values of $k_1(T,P)$ in this temperature and pressure range become available. The choice and sensitivity of the $k_1(T,P)$ parameters used in our analysis will be discussed further in the Error Analysis section.

The third-law method was used to derive the standard enthalpy for reaction 1 based on our temperature-dependent thermal decomposition rate coefficients. A summary of the obtained thermochemical data is given in Table 3. The entropy and heat capacity changes for reaction 1 were calculated using the molecular parameters listed in Table 4. The calculated entropies for NO_2 and HO_2 [$S^\circ_{298\,K}(NO_2) = 57.3$ cal mol^{-1} K^{-1} and $S^\circ_{298\,K}(HO_2) = 54.7$ cal mol^{-1} K^{-1}, respectively] are in excellent agreement with the values quoted by Sander et al.[14] The value for $\Delta_r H^\circ_{298\,K}$ was calculated from $\Delta_r H^\circ_T$ using Kirchoff's law:

$$\Delta_r H^\circ(T_2) - \Delta_r H^\circ(T_1) = \Delta_r C_P(T_2 - T_1) \qquad \text{(VII)}$$

where $\Delta_r C_P$ is the difference in heat capacity at constant pressure for reaction 1, to yield an average value of $\Delta_r H^\circ_{298\,K} = -24.0 \pm 0.5$ kcal mol^{-1} (2σ uncertainty). Values of $\Delta_f H^\circ_{298\,K}(HO_2NO_2)$, also given in Table 3, were obtained from $\Delta_r H^\circ_{298\,K}$ using the values of $\Delta_f H^\circ_{298\,K}(HO_2) = 3.3 \pm 0.8$ kcal mol^{-1} and $\Delta_f H^\circ_{298\,K}(NO_2) = 8.17 \pm 0.10$ kcal mol^{-1} quoted by Sander et al.[14] An average value of $\Delta_f H^\circ_{298\,K}(HO_2NO_2) = -12.6 \pm 1.0$ kcal mol^{-1} (2σ uncertainty) was obtained.

3.3. Error Analysis. In this section, we discuss the contributions of various possible error sources to our derived values of $k_{-1}(T,P)$, $\Delta_r H^\circ_{298\,K}$, and $\Delta_f H^\circ_{298\,K}(HO_2NO_2)$. In an effort to minimize possible systematic errors in our measurements, special attention was paid to the following key parameters: (1) the NO concentration (and its role in altering or introducing secondary reactions), (2) the temperature in the reaction zone, (3) the HO_2NO_2 concentration and, especially, its value in the reaction zone, and (4) the laser fluence that is necessary for calculating the absolute OH radical concentration.

In all of the experiments, the NO concentration was ~(2−4) × 10^{15} molecules cm^{-3}. The ratio of $[NO]/[NO_2]$ must be kept large to prevent HO_2 from reacting either with NO_2 to re-form HO_2NO_2 or with itself. In our experiments, the $[NO]/[NO_2]$ ratios were between 3 and 10 and the ratio of $k_2[NO]/k_1[NO_2][M]$ was between 30 and 200. Therefore, more than 97% of the HO_2 reacted with NO. The conversion of HO_2 to OH (reaction 2) leads to steady-state concentrations of $HO_2 < 10^{11}$ molecules cm^{-3}, as shown in the simulations, such that the HO_2 self-reaction ($k = 1.7 \times 10^{-12}$ cm^3 molecule^{-1} s^{-1}) accounted for, at most, ~2% of the HO_2 loss. Therefore, secondary reactions of the HO_2 radical did not significantly contribute to the measured value of $[OH]_{ss}$ and, hence, $k_{-1}(T,P)$.

TABLE 3: Experimentally Determined Thermochemical Data for Reaction 1 and HO_2NO_2

T (K)	P (Torr, N_2)	$k_1(T,P)^a$ (10^{-13})	$k_{-1}(T,P)$ (s^{-1})	$K_c{}^b$ (10^{-13})	$\Delta_rG°_T{}^c$ (kcal mol^{-1})	$\Delta_rS°_T$ (cal K^{-1} mol^{-1})	$\Delta_rH°_T{}^c$ (kcal mol^{-1})	$\Delta_rC_{P,T}$ (cal K^{-1} mol^{-1})	$\Delta_rH°_{298\ K}{}^c$ (kcal mol^{-1})	$\Delta_fH°_{298\ K}(HO_2NO_2)^d$ (kcal mol^{-1})
331.3	52.5	1.61	0.21 ± 0.08	7.7 ± 3.1	$-10.96^{+0.34}_{-0.22}$	−41.1	$-24.58^{+0.41}_{-0.32}$	0.791	$-24.61^{+0.41}_{-0.32}$	$-13.1^{+0.90}_{-0.87}$
331.7	25.0	0.82	0.34 ± 0.13	2.4 ± 1.0	$-10.26^{+0.36}_{-0.23}$	−41.0	$-23.81^{+0.43}_{-0.32}$	0.801	$-23.84^{+0.43}_{-0.32}$	$-12.4^{+0.91}_{-0.87}$
334.4	51.0	1.51	0.37 ± 0.14	4.1 ± 1.6	$-10.64^{+0.33}_{-0.22}$	−41.0	$-24.38^{+0.40}_{-0.32}$	0.836	$-24.41^{+0.40}_{-0.32}$	$-12.9^{+0.90}_{-0.87}$
337.9	51.3	1.46	0.73 ± 0.27	2.0 ± 0.8	$-10.26^{+0.34}_{-0.23}$	−41.0	$-24.11^{+0.41}_{-0.32}$	0.887	$-24.14^{+0.41}_{-0.32}$	$-12.7^{+0.90}_{-0.87}$
341.6	25.1	0.73	1.06 ± 0.4	0.69 ± 0.28	$-9.64^{+0.35}_{-0.24}$	−41.0	$-23.64^{+0.42}_{-0.33}$	0.917	$-23.68^{+0.42}_{-0.33}$	$-12.2^{+0.91}_{-0.87}$
342.4	53.1	1.44	1.87 ± 0.7	0.77 ± 0.3	$-9.74^{+0.34}_{-0.22}$	−41.0	$-23.78^{+0.41}_{-0.32}$	0.951	$-23.82^{+0.41}_{-0.32}$	$-12.4^{+0.90}_{-0.87}$
343.2	52.5	1.41	1.10 ± 0.4	1.28 ± 0.5	$-10.11^{+0.34}_{-0.22}$	−41.0	$-24.18^{+0.41}_{-0.32}$	0.963	$-24.22^{+0.41}_{-0.32}$	$-12.8^{+0.90}_{-0.87}$
347.3	25.1	0.68	1.47 ± 0.6	0.46 ± 0.2	$-9.51^{+0.35}_{-0.23}$	−41.0	$-23.75^{+0.42}_{-0.32}$	1.016	$-23.80^{+0.42}_{-0.32}$	$-12.3^{+0.91}_{-0.87}$
349.9	53.0	1.32	3.18 ± 1.2	0.42 ± 0.2	$-9.52^{+0.48}_{-0.28}$	−41.0	$-23.86^{+0.53}_{-0.36}$	1.049	$-23.91^{+0.53}_{-0.36}$	$-12.4^{+0.96}_{-0.88}$

[a] Units: cm^3 molecule^{-1} s^{-1}; values calculated from parameters given in Sander et al.[14] [b] Units: cm^3 molecule^{-1}. [c] Asymmetric 2σ (95% confidence limits) uncertainties based on quoted uncertainties in K_c, $\Delta_rS°_T$, $\Delta_rC_{P,T}$, $\Delta_fH_{298\ K}(HO_2)$, and $\Delta_fH_{298\ K}(NO_2)$ (see Table 5 and below). [d] $\Delta_fH_{298\ K}(HO_2NO_2) = -RT\ln(K_p) + T\Delta_rS°_T + \Delta_rC_{P,T}(298 - T) + \Delta_fH_{298\ K}(HO_2) + \Delta_fH_{298\ K}(NO_2)$, where $R = 1.987$ cal K^{-1} mol^{-1}; $K_p = K_c(RT)^{\Delta n}$, where $\Delta n = -1$ and $R = 1.363 \times 10^{-22}$ atm cm^3 molecule^{-1} K^{-1}; $\Delta_fH_{298\ K}(HO_2) = 3.3 \pm 0.8$ kcal mol^{-1} and $\Delta_fH_{298\ K}(NO_2) = 8.17 \pm 0.1$ kcal mol^{-1}, taken from Sander et al.[14] Note: 1 kcal mol^{-1} = 4.187 kJ mol^{-1} and 1 Torr = 133.3 Pa.

TABLE 4: Molecular Parameters for HO_2NO_2, NO_2, and HO_2 Used in the Calculation of Entropy and Heat Capacity

molecule	mol mass (g mol^{-1})	vibrational band energies (cm^{-1})	rotational constants (cm^{-1})	spin
$HO_2NO_2{}^a$	79.0	3540, 1728, 1397, 1304, 945, 803, 722, 654, 483, 340,[b] 310,[b] 145[b]	$A = 0.3998$ $B = 0.1555$ $C = 0.1132$	0
$HO_2{}^c$	33.0	3436, 1392, 1098	$A = 20.357$ $B = 1.118$ $C = 1.056$	$1/2$
$NO_2{}^d$	46.0	1318, 750, 1618	$A = 8.001$ $B = 0.434$ $C = 0.410$	$1/2$

[a] Vibrational band frequencies and rotational constants taken from Friedl et al.[27] unless noted. [b] Roehl et al.[6] [c] Vibrational band frequencies[28] and rotational constants from Charo and Lucia.[29] [d] Vibrational band frequencies[28] and rotational constants from Herzberg.[30]

The absolute temperature in the reaction zone where $[OH]_{ss}$ and $[HO_2NO_2]_{reactor}$ are determined is a critical parameter in determining accurate values of $k_{-1}(T,P)$. The temperature of the gas was measured using a calibrated retractable thermocouple before and after each experiment in exactly the same location where the photolysis and probe beams intersected. The temperature inside the cell was constant to within 0.2 K in the reaction volume (of about 1 cm^3). Therefore, we believe that the temperature for thermal decomposition in our experiment is accurate to within 0.2 K. The gradient in temperature between the reactor wall and the reaction zone did not contribute any error because the steady-state in OH is reached rapidly and the measured $[OH]_{ss}$ is representative of the temperature in the volume where OH was measured.

In the majority of the experiments, $[HO_2NO_2]$ was measured before and after the LIF reactor (see Table 2 and footnotes). The measured ratio of $[HO_2NO_2]_{after}/[HO_2NO_2]_{before}$ for these measurements ranged between ∼0.9 and 0.2, depending on the temperature and residence time of the gases in the reactor. (The measurements listed in Table 2 and made using UV absorption through the LIF reactor, but at similar temperatures, have slightly higher ratios; we do not attach any significance to this higher value and view it as an experimental uncertainty.) However, we do not have a direct measurement of the loss of HO_2NO_2 as a function of its location within the reactor. The HO_2NO_2 concentration in the reaction zone needed to be estimated in experiments where the HO_2NO_2 loss was significant. We have assumed, consistent with numerical simulations of the gas phase chemistry, that $[HO_2NO_2]$ decreased exponentially along the length of the reactor. We conservatively estimate that $[HO_2NO_2]_{reactor}$ was measured with an uncertainty of ∼25%. As noted earlier, the $[HO_2NO_2]_{reactor}$ estimated from the measured first-order rate coefficient for OH loss agreed (within ±30%) with the values discussed above; this agreement further supports our estimated uncertainty in $[HO_2NO_2]_{reactor}$.

The laser fluence was measured at the exit of the LIF reactor using the calibrated power meter. The power meter was calibrated in a separate set of experiments, as described in the Experimental Section. We estimate the uncertainty of this calibration to be ∼10% at the 95% confidence level.

The uncertainties in the quantities described above contribute to the uncertainties in the calculated values of $\Delta_rH°_{298\ K}$ and $\Delta_fH°_{298\ K}(HO_2NO_2)$. The overall uncertainties in $\Delta_rH°_{298\ K}$ and $\Delta_fH°_{298\ K}(HO_2NO_2)$ were obtained by propagating the errors sequentially in $[OH]_{ss}$, $k_{-1}(T,P)$, K_c, K_p, and the thermodynamic quantities. The uncertainties in each of these quantities and the parameters used in their calculation are given in Table 5. We calculated the uncertainty in the $[OH]_{ss}$ measurement to be 25%. Using the uncertainties for $[HO_2NO_2]$ quoted in Table 5, we estimate the uncertainty in $k_{-1}(T,P)$ to be ∼35%. Kurylo and Ouellette[12] report uncertainties in the measured values of $k_1(T,P)$ at 25 and 50 Torr to be <25%. Their rate coefficient, k_1(300 K, 50 Torr) = $(2.32 \pm 0.56) \times 10^{-13}$ cm^3 molecule^{-1} s^{-1}, differs from the value derived by Sander and Peterson,[11] k_1(300 K, 50 Torr) = $(3.05 \pm 0.53) \times 10^{-13}$ cm^3 molecule^{-1} s^{-1}. Recently, Christensen et al.[25] measured the rate coefficients for reaction 1 from 220 to 298 K and from 45 to 200 Torr of N_2. These measurements were made in the same laboratory as that of Sander and Peterson and yield values of $k_1(T,P)$ that agree with the values from Kurylo and Ouellette (within 5%) under our temperature and pressure conditions. This good agreement ensures us that the uncertainties in $k_1(T,P)$ for our calculation are no more than 20%.

We estimate the uncertainty (2σ, 95% confidence limit) for K_c to be ∼40%. Assuming the uncertainty for temperature measurement and entropy and heat capacity calculations of 0.06%,

TABLE 5: Estimated Uncertainties Used in the Derivation of the Overall Uncertainty of $\Delta_rH°_{298\,K}$ for Reaction 1 and $\Delta_fH°_{298\,K}(HO_2NO_2)$

	uncertainty (2σ, 95% confidence level)	
quantities	relative (%)	absolute/source
power meter calibration	±10	$\pm 1 \times 10^{14}$ photons cm^2 mJ^{-1}
H_2O_2 absorption cross section	±15	$\pm 1.35 \times 10^{-20}$ cm^2 molecule^{-1}
laser power measurement	±10	±0.3 mJ cm^{-2}
S_{OH}^{PNA}	±5	2×10^9 molecules cm^{-3}
$S_{OH}^{H_2O_2}$	±5	2×10^9 molecules cm^{-3}
$[OH]_{ss}$	±25	
k_3'	±5	±100 s^{-1}
[PNA]	±25	$\pm 0.1 \times 10^{15}$ molecules cm^{-3}
$k_{-1}(T,P)$	±35	derived from $[OH]_{ss}$, k_3' and [PNA]
$k_1(T,P)$	±20	analysis of literature values
$K_p(T)$	±40	derived from $k_{-1}(T,P)$ and $k_1(T,P)$
temperature	±0.06	±0.2 K
$S°_T(HO_2NO_2)$	±0.9	±0.7 cal K^{-1} mol^{-1}
$\Delta_rC_P(T)$	±10	±0.1 cal K^{-1} mol^{-1}

3%, and 3%, respectively, we calculate the overall uncertainty for $\Delta_rH°_{298\,K}$ to be ±0.5 kcal mol^{-1} and $\Delta_fH°_{298\,K}(HO_2NO_2)$ to be ±1.0 kcal mol^{-1} where the uncertainties are at the 95% confidence level.

Figure 5 shows the temperature dependence of the equilibrium constant $K_p(T)$ given in Table 3. Only the lowest temperature data point measured at 25 Torr shows a significant deviation of $K_p(T)$ from the van't Hoff relationship. Figure 6 shows the calculated $\Delta_fH°_{298\,K}(HO_2NO_2)$ dependence on temperature and pressure. As shown in Figure 6a, there is no dependence of $\Delta_fH°_{298\,K}(HO_2NO_2)$ derived from the data over the temperature range used in this work. The value of $\Delta_fH°_{298\,K}(HO_2NO_2)$ at 25 Torr (see Figure 6b) is perhaps slightly systematically different from that at 50 Torr. This could be partly due to a systematic error in k_1 taken from the literature. If we calculate $\Delta_fH°_{298\,K}(HO_2NO_2)$ at 25 and 50 Torr separately, we obtain -12.3 ± 0.2 kcal mol^{-1} (3 data points) and -12.7 ± 0.6 kcal mol^{-1} (6 data points), respectively, where the uncertainties are 2σ. These two values agree well within the combined errors. The difference may indicate a small systematic dependence of our thermal decomposition rate coefficient determination on pressure.

3.4. Comparison with Previous Studies. Because of the differences in temperatures and pressures used, it is not possible to directly compare the thermal decomposition rate coefficients $k_{-1}(T,P)$ measured in our study with those measured by Graham et al.[2,3] and Zabel.[4] Therefore, we have chosen to compare the values of $\Delta_rH°_{298\,K}$ derived from the thermal decomposition rate coefficient data. It is better to compare $\Delta_rH°_{298\,K}$ rather than $\Delta_fH°_{298\,K}(HO_2NO_2)$ because the former does not depend on the values of $\Delta_fH°_{298\,K}(NO_2)$ and $\Delta_fH°_{298\,K}(HO_2)$. These values, especially $\Delta_fH°_{298\,K}(HO_2)$, have been changed markedly in the past 15 years. However, the determination of $\Delta_rH°_{298\,K}$ does require an evaluation of $\Delta_rS°_{298\,K}$.

Graham et al.[2,3] and Zabel[4] measured, using essentially identical experimental methods, the HO_2NO_2 thermal decomposition rate coefficients currently available. They used temperature controlled reaction chambers equipped with multipass Fourier transform infrared absorption to monitor the loss of HO_2NO_2 in the presence of high concentrations of NO. The high concentration of NO rapidly converted HO_2 to OH via reaction 2 and suppressed re-formation of HO_2NO_2 via reaction 1. OH radicals produced in their system were mostly removed via reactions with NO and NO_2. However, the conditions used in the Graham et al.[3] study were not sufficient to eliminate HO_2NO_2 loss via reaction with OH. Using the recent rate coefficient for the OH + HO_2NO_2 reaction from Jiménez et al.,[10] a reanalysis of the data of Graham et al. reduces their reported thermal decomposition rate coefficients by approximately 25% (at all temperatures and pressures). In the Zabel[4]

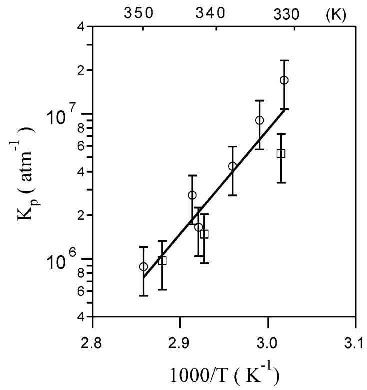

Figure 5. Temperature dependence of the equilibrium constant $K_p(T)$ derived in this work using our measured $k_{-1}(T,P)$ values and literature values of $k_1(T,P)$ (see text for details). The experimental data were recorded at 50 Torr (N_2) (circles) and 25 Torr (N_2) (squares). The solid line is a weighted least-squares fit of the data.

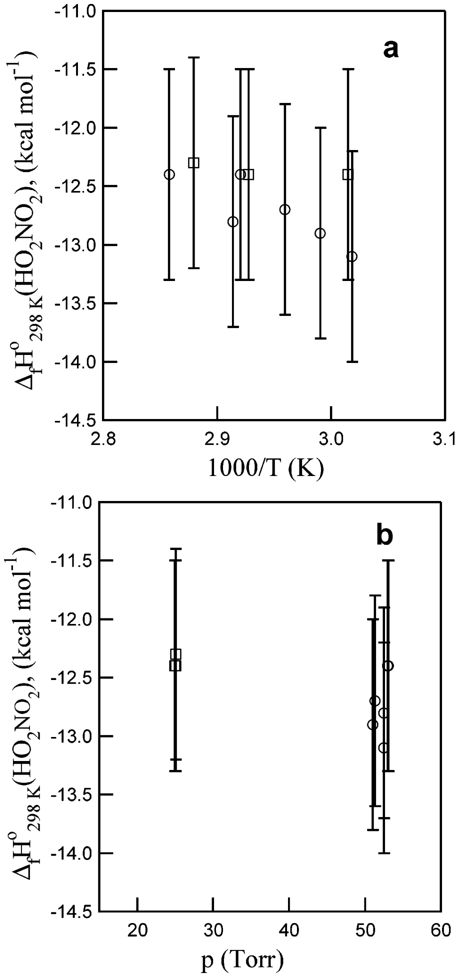

Figure 6. Values of $\Delta_fH_{298\,K}(HO_2NO_2)$ determined in this work plotted against the experimental temperature (a) and pressure (b) used in the measurements. The data obtained at 25 Torr (N_2) are shown as squares and the 50 Torr (N_2) data as circles. The error bars are taken from the analysis given in Table 5.

study, the measured HO_2NO_2 depletion rate was not significantly influenced by loss via its reaction with OH; that is, it truly reflected $k_{-1}(T,P)$. Graham et al. measured $k_{-1}(T,P)$ between 261 and 295 K with N_2 or O_2 pressures between 1 and 760 Torr. Zabel[4] measured $k_{-1}(T,P)$ between 261 and 307 K with N_2 pressures between 10 and 770 Torr. Although the rate coefficients of Graham et al. [3] and Zabel[4] agree within their combined error limits, extrapolation of their data to temperatures and pressures typical of the upper troposphere yield values that differ by a factor of ~2.

The equilibrium constant as a function of temperature can be analyzed for $\Delta_rH°$ using either the second-law method (van't Hoff analysis) or third-law method. Previous reports have used the second-law analysis, where the slope of a plot of $\ln(K_p)$ versus $1/T$ yields $\Delta_rH°$ (at the median temperature). However, because K_p is usually determined over a limited temperature range, because of experimental constraints, the obtained value of $\Delta_rH°$ could have large errors; that is, there is a correlation between $\Delta_rH°$ and $\Delta_rS°$. The entropy of reaction $\Delta_rS°$ can now be calculated more accurately using statistical thermodynamics than it can by an extrapolation of the van't Hoff plot. Using the third-law method, as done in this work, therefore reduces the uncertainty in $\Delta_rH°$.

Statistical thermodynamic calculations of $S°_{298\,K}$ for HO_2, NO_2, and HO_2NO_2 provide the most accurate method for the determination of $\Delta_rS°_{298\,K}$ for reaction 1. The availability of accurate molecular parameters (vibrational frequencies and rotational constants) for each of these species makes the calculated $\Delta_rS°_{298\,K}$ more accurate than current experimental determinations. The calculations presented in this work yield $\Delta_rS°_{298\,K} = -41.1$ cal mol^{-1} K^{-1} where $S°_{298\,K}(HO_2) = 54.8$ cal mol^{-1} K^{-1}, $S°_{298\,K}(NO_2) = 57.4$ cal mol^{-1} K^{-1}, and $S°_{298\,K}(HO_2NO_2) = 71$ cal mol^{-1} K^{-1} (see Table 6). The results for HO_2NO_2 compare very well with the similarly calculated value of Chen and Hamilton[26] [$S°_{298\,K}(HO_2NO_2) = 71.1$ cal mol^{-1} K^{-1}] and the average value of $S°_{298\,K}(HO_2NO_2) = 70.3 \pm 0.7$ cal mol^{-1} K^{-1} reported by Regimbal and Mozurkewich.[13] The difference of 0.8 cal mol^{-1} K^{-1} between the two calculated values is also roughly the uncertainty quoted by Regimbal and Mozurkewich; this difference results mostly from the differing treatment of the ν_2 vibrational torsion in HO_2NO_2. The larger value of $S°_{298\,K}(HO_2NO_2)$ is obtained by taking the ν_2 frequency to be 310 cm^{-1}, as done in our calculation. Note that this vibrational band has not been observed experimentally and the frequency is obtained from ab initio calculations. Regimbal and Mozurkewich calculated a lower limit for $S°_{298\,K}(HO_2NO_2)$ of 69.3 cal mol^{-1} K^{-1} by treating the ν_2 vibration as a hindered rotor. We have used our calculated $S°_{298\,K}(HO_2NO_2)$ (using a low frequency torsion) but have adopted the estimated error in $\Delta_rS°_{298\,K}$ to be ± 0.7 cal mol^{-1} K^{-1} in the error analysis given above and in Table 5. It is worth noting that this difference is still much smaller than the uncertainty in $\Delta_rS°_{298\,K}$ obtained using the van't Hoff analysis. The previous experimental determinations of $\Delta_rS°_{298\,K}$ are in reasonable agreement, within their quoted uncertainties, with our value; see Table 6 for a comparison. In the discussion of $\Delta_rH°_{298\,K}$ to follow, we need to keep in mind the significance of differences in $\Delta_rS°_{298\,K}$ when comparing values reported in the literature. To enable a more direct comparison of experimental values, Table 6 also contains $\Delta_rH°_{298\,K}$ values obtained from a reanalysis of the reported kinetic data using $\Delta_rS°_{298\,K} = -41.1$ cal mol^{-1} K^{-1} and the currently recommended values of $k_1(T,P)$ where possible.

A summary of the thermodynamic values obtained in this work together with those obtained by others is given in Table

TABLE 6: Summary of Reported Thermodynamic Parameters for HO_2NO_2 (PNA) and $HO_2 + NO_2 \leftrightarrow HO_2NO_2$, Reaction 1[a]

$S°_{298\,K}(NO_2)$	$S°_{298\,K}(HO_2)$	$S°_{298\,K}$(PNA)	$\Delta_fH°_{298\,K}(NO_2)$	$\Delta_fH°_{298\,K}(HO_2)$	$\Delta_fH°_{298\,K}$(PNA)	$\Delta_rH°_{298\,K}$	$\Delta_fH°_{298\,K}{}^a$(PNA)	$\Delta_rH°_{298K}{}^a$	$\Delta_rS°_{298K}$	reference	method
		76.2					-12.4^b	-23.9^b	−35.4	Cox and Patrick[31]	calculation: based on rate coefficient pre-exponential factors
57.4	54.8	71.9	7.9	2.5	−13.7	− 24.1	-12.7^c	-24.2^c	−40.3	Golden and co-workers[32,33]	calculation: RRKM theory
		73.8 ± 2			−12.6±2	−23.0	-12.7^d	-24.2^d	−37.9	Sander and Peterson[11]	second-law analysis
		71.4^e			-12.3^e	−23.8 ± 0.7	-12.5^f	-24.0^f	−40.7	Zabel[4]	second-law analysis
		71.1				−22				Chen and Hamilton[26]	calculation: ab initio
57.4	54.8	70.3 ± 0.7			−12.9 ± 0.6					Regimbal and Mozurkewich[13]	liquid-phase decomposition with calculated entropy
57.4	54.8	70.3 ± 0.7	8.17 ± 0.1	3.3 ± 0.8	−12.7 ± 0.6					Sander et al.[14]	data compilation
57.4	54.8	71.0 ± 0.7	8.17 ± 0.1	3.3 ± 0.8	−12.6 ± 1.0	−24.0 ± 0.5			−41.1	this work	third-law analysis

[a] Units: $S°$ in cal mol^{-1} K^{-1} and $\Delta H°$ in kcal mol^{-1}; 1 kcal mol^{-1} = 4.187 kJ mol^{-1}. Recalculated thermodynamic parameters using the currently derived values of $\Delta_rS°_{298\,K}$ and the enthalpies and entropies of NO_2 and HO_2 quoted in Sander et al.[14] (see footnotes for details specific to each study). [b] Calculated using our $k_{-1}(T,P)$ and $k_1(T,P)$ from their work measured at 283 K and adjusted to 298 K using the temperature factor from Kurylo and Ouellette.[12] [c] Calculated using their calculated K_c at 298 K. [d] Calculated using K_c calculated from their $k_1(T,P)$ and Graham et al.[3] thermal decomposition data with a 25% reduction to account for the OH + HO_2NO_2 reaction (see text for details). [e] Calculated from their $\Delta_rH°_{298\,K}$ and $\Delta_rS°_{298\,K}$. [f] Calculated using K_p from a fit of K_p versus $1/T$ data reported in his work.

6. Sander and Peterson[11] used their $k_1(T,P)$ values with the $k_{-1}(T,P)$ values from Graham et al.[3] to obtain $\Delta_r S°_{298\,K} = -37.9$ cal mol^{-1} K^{-1} and $\Delta_r H°_{298\,K} = -23.0$ kcal mol^{-1}; these are only in modest agreement with the values obtained in our study. Zabel[4] used $k_1(T,P)$ values from Kurylo and Ouellette[12] and his $k_{-1}(T,P)$ values and obtained $\Delta_r H°_{298\,K}$ and $\Delta_r S°_{298\,K}$ values for reaction 1 in good agreement with our results. Regimbal and Mozurkewich[13] have reported $S°_{298\,K}(HO_2NO_2) = 70.3 \pm 0.7$ cal K^{-1} mol^{-1} and $\Delta_f H°_{298\,K}(HO_2NO_2) = -12.9 \pm 0.6$ kcal mol^{-1}. Their values are in good agreement with our work. Note that the methods used in the $\Delta_f H°_{298\,K}(HO_2NO_2)$ determination by Regimbal and Mozurkewich and those used in this work differ significantly. The values of $\Delta_f H°_{298\,K}$ and $\Delta_f H°_{298\,K}(HO_2NO_2)$ obtained in this work are also in good agreement with the recalculated values from previous studies.

On the basis of the above discussion, we recommend $\Delta_r H°_{298\,K} = -24.0 \pm 0.5$ kcal mol^{-1} and $\Delta_f H°_{298\,K}(HO_2NO_2) = -12.6 \pm 1.0$ kcal mol^{-1}. These values are an average of the values derived in this work and values recalculated from previous works using currently recommended $k_1(T,P)$ rate coefficient data and $S°_{298\,K}(HO_2NO_2) = 71.0$ cal mol^{-1} K^{-1}. The quoted uncertainties are at the 95% confidence level.

3.5. Implications to the Atmosphere. The formation of HO_2NO_2 leads to a temporary reservoir for NO_x, and possibly also for HO_x. HO_2NO_2 is removed from the atmosphere via thermal decomposition, photolysis (in the UV or in the visible/near-IR), and reaction with OH. All three removal processes regenerate NO_x in the atmosphere; however, the reaction of OH with HO_2NO_2 leads to a net destruction of HO_x. To evaluate the role of HO_2NO_2 in determining HO_x abundances, it is therefore necessary to know the relative rates of these processes in the atmosphere. Also, to calculate the abundance of HO_2NO_2 in the atmosphere and the extent to which HO_2NO_2 acts as a NO_x reservoir, it is necessary to know the sum of the rate coefficients for the removal of HO_2NO_2.

The rate coefficient $k_{-1}(T,P)$ for the thermal decomposition of HO_2NO_2 is very slow under the conditions of the upper troposphere. The thermal decomposition lifetime of HO_2NO_2 changes very rapidly with temperature such that, for temperatures less than 250 K, the other HO_2NO_2 loss processes discussed above control its atmospheric lifetime. However, it is difficult to measure $k_{-1}(T,P)$ under the atmospheric conditions where the transition in the dominance of loss processes occurs. Consequently, one needs to use the measured value for the rate coefficient for the formation of HO_2NO_2 along with thermochemical data to calculate the thermal decomposition rate coefficient. However, even a small error in $\Delta_r H°_{298\,K}$ for the reaction leads to a large uncertainty in $k_{-1}(T,P)$. For example, an uncertainty of 0.5 kcal mol^{-1} in $\Delta_r H°_{298\,K}$ (as obtained in this work) leads to an uncertainty of a factor of more than 3 in the calculated value of $k_{-1}(T,P)$. Therefore, one needs to either greatly reduce the uncertainty in $\Delta_r H°_{298\,K}$ or, ideally, measure $k_{-1}(T,P)$ under the appropriate atmospheric conditions. The value of $\Delta_r H°_{298\,K}$ determined in this work and the values of $k_{-1}(T,P)$ derived for relevant atmospheric conditions are the most accurate to date.

Until now in the discussion, we have assumed that HO_2NO_2 thermally decomposes to yield only HO_2 and NO_2. However, PNA may also thermally dissociate to give HONO + O_2 as products

$$HO_2NO_2 \rightarrow HONO + O_2 \qquad (-1b)$$

where $\Delta_r H°_{298\,K} = -6.4$ kcal mol^{-1}. This reaction, which is exothermic, is believed to be slow because of a large barrier. In our experiments, we are "blind" to this channel because the first-order decomposition rate coefficient measured is only for the channel that produces HO_2. However, the UV absorption spectra of the sample after the reactor indicate that less than 10% of the HO_2NO_2 lost via thermal decomposition in the reactor is converted to HONO. The value of $k_{-1}(T,P)$ measured by Graham et al.[3] and Zabel[4] is the sum of the rate coefficients for the channels that yield $HO_2 + NO_2$ and HONO + O_2. The good agreement in the value of $\Delta_r H°_{298\,K}$ derived by us, on the one hand, and that of Graham et al. and Zabel, on the other hand, suggests that channel −1b is not very important. It is worth noting, however, that a heterogeneous conversion of HO_2NO_2 to HONO may be possible with some significant consequences to HO_x production.

Acknowledgment. This work was supported in part by NOAA's Health of the Atmosphere Research Program.

References and Notes

(1) Salawitch, R. J.; Wennberg, P. O.; Toon, G. C.; Sen, B.; Blavier, J. F. *Geophys. Res. Lett.* **2002**, *29*, 10.1029/2002GL015006.
(2) Graham, R. A.; Winer, A. M.; Pitts, J. N., Jr. *Chem. Phys. Lett.* **1977**, *51*, 215.
(3) Graham, R. A.; Winer, A. M.; Pitts, J. N., Jr. *J. Phys. Chem.* **1978**, *68*, 4505.
(4) Zabel, F. *Z. Phys. Chem. (Muenchen)* **1995**, *188*, 119.
(5) MacLeod, H.; Smith, G. P.; Golden, D. M. *J. Geophys. Res.* **1988**, *93*, 3813.
(6) Roehl, C. M.; Mazely, T. L.; Friedl, R. R.; Li, Y.; Francisco, J. S.; Sander, S. P. *J. Phys. Chem. A* **2001**, *105*, 1592.
(7) Roehl, C. M.; Nizkorodov, S. A.; Zhang, H.; Blake, G. A.; Wennberg, P. O. *J. Phys. Chem. A* **2002**, *106*, 3766.
(8) Jimenez, E.; Gierczak, T.; Stark, H.; Burkholder, J. B.; Ravishankara, A. R. *Phys. Chem. Chem. Phys.* **2004**, in press.
(9) Smith, C. A.; Molina, L. T.; Lamb, J. J.; Molina, M. J. *Int. J. Chem. Kinet.* **1984**, *16*, 41.
(10) Jiménez, E.; Gierczak, T.; Stark, H.; Burkholder, J. B.; Ravishankara, A. R. *J. Phys. Chem. A* **2004**, *108*, 1139.
(11) Sander, S. P.; Peterson, M. E. *J. Phys. Chem.* **1984**, *88*, 1566.
(12) Kurylo, M. J.; Ouellette, P. A. *J. Phys. Chem.* **1987**, *91*, 3365.
(13) Regimbal, J. M.; Mozurkewich, M. *J. Phys. Chem. A* **1997**, *101*, 8822.
(14) Sander, S. P.; Finlayson-Pitts, B. J.; Friedl, R. R.; Golden, D. M.; Huie, R. E.; Kolb, C. E.; Kurylo, M. J.; Molina, M. J.; Moortgat, G. K.; Orkin, V. L.; Ravishankara, A. R. *Chemical Kinetics and Photochemical Data for Use in Atmospheric Studies, Evaluation Number 14*; JPL Publication 02-25; Jet Propulsion Laboratory: Pasadena, CA, 2002.
(15) Vaghjiani, G. L.; Ravishankara, A. R.; Cohen, N. *J. Phys. Chem.* **1989**, *93*, 7833.
(16) Gierczak, T.; Burkholder, J. B.; Talukdar, R. K.; Mellouki, A.; Barone, S. B.; Ravishankara, A. R. *Int. J. Chem. Kinet.* **1997**, *110*, 1.
(17) Schneider, W.; Moortgat, G. K.; Tyndall, G. S.; Burrows, J. P. *J. Photochem. Photobiol., A* **1987**, *40*, 195.
(18) Ravishankara, A. R.; Wine, P. H.; Nicovich, J. M. *J. Phys. Chem.* **1983**, *78*, 6629.
(19) Smith, C. A. The Atmospheric Reaction Kinetics of OH by Flash Photolysis−Resonance Fluorescence. Ph.D. Thesis, University of California, Berkeley, CA, 1983.
(20) Rothman, L. S.; Rinsland, C. P.; Goldman, A.; Massie, S. T.; Edwards, D. P.; Flaud, J.-M.; Perrin, A.; Camy-Peyret, C.; Dana, V.; Mandin, J.-Y.; Schroeder, J.; McCann, A.; Gamache, R. R.; Wattson, R. B.; Yoshino, K.; Chance, K. V.; Jucks, K. W.; Brown, L. R.; Nemtchinov, V.; Varanasi, P. *J. Quant. Spectrosc. Radiat. Transfer* **1998**, *60*, 665.
(21) Kegley-Owen, C. S.; Gilles, M. K.; Burkholder, J. B.; Ravishankara, A. R. *J. Phys. Chem. A* **1999**, *103*, 5040.
(22) Knight, G.; Ravishankara, A. R.; Burkholder, J. B. *Phys. Chem. Chem. Phys.* **2002**, *4*, 1432.
(23) Kenley, R. A.; Trevor, P. L.; Lan, B. Y. *J. Am. Chem. Soc.* **1981**, *103*, 2203.
(24) Kurylo, M. J.; Ouellette, P. A. *J. Phys. Chem.* **1986**, *90*, 441.
(25) Christensen, L. E.; Okumura, M.; Sander, S. P.; Friedl, R. R.; Miller, C. E.; Sloan, J. J. *J. Phys. Chem. A* **2004**, *108*, 80.
(26) Chen, Z.; Hamilton, T. P. *J. Phys. Chem.* **1996**, *100*, 15731.
(27) Friedl, R. R.; May, R. D.; Duxbury, G. *J. Mol. Spectrosc.* **1994**, *165*, 481.

(28) *NIST Chemistry WebBook*; NIST Standard Reference Database Number 69; Linstrom, P. J., Mallard, W. G., Eds.; National Institute of Standards and Technology: Gaithersburg, MD, 2003. http://webbook.nist.gov.

(29) Charo, A.; Lucia, F. D. *J. Mol. Spectrosc.* **1982**, *94*, 426.

(30) Herzberg, G. *Electronic Spectra and Electronic Structure of Polyatomic Molecules*; Van Nostrand: New York, 1966.

(31) Cox, R. A.; Patrick, K. *Int. J. Chem. Kinet.* **1979**, *11*, 635.

(32) Baldwin, A. C.; Golden, D. M. *J. Phys. Chem.* **1978**, *82*, 644.

(33) Patrick, R.; Golden, D. M. *Int. J. Chem. Kinet.* **1983**, *15*, 1189.